Nanoparticles enhance brain delivery of blood–brain barrier-impermeable probes for in vivo optical and magnetic resonance imaging

Robert M. Koffie[a,b], Christian T. Farrar[c], Laiq-Jan Saidi[a], Christopher M. William[a], Bradley T. Hyman[a], and Tara L. Spires-Jones[a,1]

[a]Department of Neurology, Massachusetts General Hospital and Harvard Medical School, Charlestown, MA 02129; [b]Harvard Biophysics Program, Harvard University, Boston, MA 02115; and [c]Athinoula A. Martinos Center for Biomedical Imaging, Department of Radiology, Massachusetts General Hospital and Harvard Medical School, Charlestown, MA 02129

Edited by William Klunk, University of Pittsburgh, Pittsburgh, PA, and accepted by the Editorial Board October 12, 2011 (received for review July 18, 2011)

Several imaging modalities are suitable for in vivo molecular neuroimaging, but the blood–brain barrier (BBB) limits their utility by preventing brain delivery of most targeted molecular probes. We prepared biodegradable nanocarrier systems made up of poly(n-butyl cyanoacrylate) dextran polymers coated with polysorbate 80 (PBCA nanoparticles) to deliver BBB-impermeable molecular imaging probes into the brain for targeted molecular neuroimaging. We demonstrate that PBCA nanoparticles allow in vivo targeting of BBB-impermeable contrast agents and staining reagents for electron microscopy, optical imaging (multiphoton), and whole brain magnetic resonance imaging (MRI), facilitating molecular studies ranging from individual synapses to the entire brain. PBCA nanoparticles can deliver BBB-impermeable targeted fluorophores of a wide range of sizes: from 500-Da targeted polar molecules to 150,000-Da tagged immunoglobulins into the brain of living mice. The utility of this approach is demonstrated by (*i*) development of a "Nissl stain" contrast agent for cellular imaging, (*ii*) visualization of amyloid plaques in vivo in a mouse model of Alzheimer's disease using (traditionally) non–BBB-permeable reagents that detect plaques, and (*iii*) delivery of gadolinium-based contrast agents into the brain of mice for in vivo whole brain MRI. Four-dimensional real-time two-photon and MR imaging reveal that brain penetration of PBCA nanoparticles occurs rapidly with a time constant of ∼18 min. PBCA nanoparticles do not induce nonspecific BBB disruption, but collaborate with plasma apolipoprotein E to facilitate BBB crossing. Collectively, these findings highlight the potential of using biodegradable nanocarrier systems to deliver BBB-impermeable targeted molecular probes into the brain for diagnostic neuroimaging.

in vivo multiphoton imaging | transgenic mice

The ability to image structure and function in the brain using tools as diverse as multiphoton fluorescence imaging and magnetic resonance imaging (MRI) hold the promise of providing insight into physiology and pathophysiological conditions, but are greatly limited by the ability to deliver contrast agents with molecular specificity across the blood–brain barrier (BBB). Although several molecular imaging contrast agents targeted to structures of interest have been developed for research and clinical applications, only a small fraction of them cross the BBB, including amyloid binding dyes that required many years to develop (1–4). This leads to surprising gaps in the ability to monitor cells and cellular processes in the central nervous system (CNS), requiring skull burr holes and topical application to visualize agents ranging from simple molecular Nissl stains to highly specific antibodies (5–7). Multiple approaches have been developed to nonspecifically disrupt the BBB to allow BBB-impermeable targeted molecular imaging probes entrance into brain parenchyma, but these approaches induce uncontrolled neuronal injuries as well as allow circulating toxins and neuroactive agents to get into the brain (8). There is therefore a growing need to devise effective and safe ways to selectively deliver BBB-impermeable targeted molecular imaging probes into the brain for in vivo diagnostic molecular neuroimaging.

Biodegradable nanoparticles (NPs) are promising carrier systems for brain delivery of exogenous molecules (9). Among the various brain delivery nanocarrier systems devised over the years, polysorbate 80-coated poly(n-butyl cyanoacrylate) (PBCA) NPs show tremendous promise. PBCA NPs have been explored to deliver a number of BBB-impermeable drugs including growth factors, antiepileptics, and chemotherapeutic agents into the brain of animals with varying success (10–14). Most studies demonstrating use of PBCA NPs to deliver exogenous agents into the brain, however, rely on secondary assessment of drug efficacy or postmortem examination of brain tissue to ascertain BBB crossing; direct real-time visualization of PBCA nanocarriers crossing the BBB in living animals was previously unexplored, making it difficult to determine whether this nanoparticulate approach could be used for live in vivo diagnostic imaging of dynamic CNS processes in living animals.

In this work, we investigate the potential of using PBCA NPs to deliver BBB-impermeable molecular imaging contrast agents and biologics into the brain of mice for in vivo multiphoton microscopy and MRI. First, we use PBCA NPs to deliver three well-known BBB-impermeable fluorophores for in vivo imaging: one for imaging nuclei in the brain of wild-type mice and another two for imaging neuropathological changes of Alzheimer's disease (AD) in transgenic mouse models. Second, using four-dimensional (4D) real-time two-photon in vivo microscopy, we explore the kinetics of PBCA NP-mediated delivery of one of these fluorophores in the brain of living intact animals. Third, we demonstrate that PBCA NPs can be used to deliver not only fluorophores into the brain for optical imaging, but therapeutic antibodies and MR contrast agents as well. Finally, we explore the mechanism by which PBCA NPs cross the BBB and show that PBCA NPs do not nonspecifically disrupt the BBB, but instead use endogenous lipidated apolipoprotein E particles to facilitate BBB crossing. From the scale of nanometer gold particles detected by transmission electron microscopy (TEM) postmortem, through micrometer resolution using in vivo two-photon microscopy in animals with a craniotomy, all of the way to MR imaging in completely intact animals, we were able to observe the movement of compounds bound to NPs into the brain parenchyma without a global

Author contributions: R.M.K., B.T.H., and T.L.S.-J. designed research; R.M.K., C.T.F., L.-J.S., C.M.W., and T.L.S.-J. performed research; R.M.K. and C.T.F. analyzed data; and R.M.K., B.T.H., and T.L.S.-J. wrote the paper.

The authors declare no conflict of interest.

This article is a PNAS Direct Submission. W.K. is a guest editor invited by the Editorial Board.

[1]To whom correspondence should be addressed. E-mail: tspires@partners.org.

This article contains supporting information online at www.pnas.org/lookup/suppl/doi:10.1073/pnas.1111405108/-/DCSupplemental.

disruption of the BBB. Collectively, our results demonstrate that PBCA NPs can be used as effective nanocarriers to enhance delivery of BBB-impermeable targeted molecular imaging probes for in vivo optical and MR imaging of the brain.

Results

To determine whether PBCA NPs coated with polysorbate 80 can effectively deliver molecular imaging probes into the brain of living animals, we synthesized PBCA NPs encapsulated with different molecular imaging fluorophores (Fig. S1 for characterization), administered them i.v. into mice, and imaged the first several hundred micrometers of cortex in vivo using intravital multiphoton microscopy through a craniotomy sealed with a glass coverslip. We first explored nanoparticle-assisted brain delivery of a small polar DNA-binding dye bis-benzimide (Hoechst 33258, 531.86 Da M_r; Fig. S2 for structure). Previously, we have confirmed this dye as useful for monitoring neuronal nuclei in vivo despite its tendency to photobleach, but it previously required topical application to the brain because it does not cross the BBB, precluding longitudinal imaging (15). We confirmed that Hoechst 33258 alone dissolved in saline does not cross the BBB when administered i.v. (Fig. 1*A* and Movie S1). On the contrary, in vivo two-photon microscopy of cortical layers I–II of living anesthetized mice i.v. injected with Hoechst 33258 encapsulated in polysorbate 80-coated PBCA NPs reveals robust Hoechst fluorescence in a pattern of neuronal/glial nuclei beginning 30 min after injection, peaking at 24 h, and persisting for 2 d ($n = 8$ mice) (Fig. 1*B* and Movie S1). Postmortem imaging of brain slices of animals not subjected to cranial window surgery revealed robust nuclear staining throughout the brain in cohorts injected with Hoechst adsorbed onto PBCA NPs, but not those injected with Hoechst alone (Fig. S3), suggesting that PBCA NP-mediated delivery of Hoechst into the brain is not an artifact of cranial window surgery or imaging. PBCA NPs did not induce toxic histopathological changes or overt physical distress in injected mice (Fig. S4).

Next, we explored the use of PBCA NPs as nanocarriers for delivering targeted probes for imaging neuropathological lesions of a neurodegenerative disease in living mice. Alzheimer's disease is characterized histopathologically by the deposition of neuritic plaques made up of amyloid-beta (Aβ) peptides and neurofibrillary tangles (NFTs) composed of hyperphosphorylated tau protein (16). Significant progress has been made in developing imaging modalities for visualizing amyloid plaques in vivo with BBB-permeable agents including Pittsburgh compound B and methoxy XO4 (1, 3). However, synthesizing additional BBB-permeable high-affinity contrast agents that specifically stain NFTs or soluble oligomeric Aβ, which are believed to be the most toxic species in the brain of AD patients (17–20), remains elusive. We synthesized PBCA NPs using dextran (70,000 Da M_r) covalently conjugated to Texas red (TX-red-Dx), a molecular imaging dye that binds senile plaques ex vivo, but is routinely used to generate fluorescence angiograms during in vivo intravital imaging due to its long vascular half-life and BBB impermeability. We confirm that TX-red-Dx alone did not cross the BBB in 6-mo-old AD transgenic mice ($n = 6$, $APP_{swe}/PS1_{deltaE9}$) and remained in blood vessels even 2 h following i.v. injection (Fig. 2*A* and Movie S2). Nanoparticulate integration of TX-red-Dx and polysorbate-80 coating, however, allowed it to cross the BBB, labeling cerebral amyloid angiopathy (CAA), amyloid plaques, and glial/neuronal cell bodies ($n = 6$ mice; Fig. 2 *B* and *C* and Movie S2) 2 h after i.v. administration. NP-conjugated TX-red-Dx moved across the BBB to stain CNS cell bodies, CAA, and plaques, resulting in a dramatic ~45% decrease in fluorescence intensity in blood vessels within 1 h after i.v. injection compared with only a ~5% decrease in fluorescence intensity upon injecting TX-red-Dx unincorporated into PBCA NPs.

To further explore the potential of using PBCA NPs to deliver targeted molecular imaging dyes that are noncovalently adsorbed onto nanoparticles for imaging AD neuropathological changes in vivo, we synthesized NPs loaded with Trypan blue (M_r 872.9 Da), a plaque-binding red fluorescing diazo dye that is well documented not to cross the BBB (21, 22). We first confirmed through confocal imaging of postmortem brain slices that i.v. administration of Trypan blue adsorbed onto PBCA NPs crosses the BBB and specifically labels senile plaques in the brain of APP/PS1 mice ($n = 5$) after 2 h of injection, but not Trypan blue administered alone in saline (Fig. S5). Trypan blue fluorescence is not dependent on target binding, making it particularly suitable for kinetic studies. We therefore studied the kinetics of PBCA NP-mediated Trypan blue delivery into the brain of APP/PS1 mice using in vivo 4D two-photon microscopy and found that the fluorophore had a circulating half-life of 60.6 ± 8.2 min when adsorbed onto PBCA NPs (Fig. 3). Trypan blue fluorescence signal in amyloid plaques was first detectable above noise within 10 min after injection and increased progressively, peaking at ~2 h following i.v. administration of PBCA NPs with penetrating and plaque-binding time constants of 18.0 ± 2.3 and 59.6 ± 6.9 min, respectively (kinetics follow Boltzmann's model equation) (Fig. 3*B* and Movie S3). Because in vivo two-photon microscopy only allows visualization of tissue <400 μm deep, we also carried out postmortem analysis of brain slices after kinetic studies and confirmed that amyloid plaques throughout cortical and subcortical regions of APP/PS1 mice are robustly stained with Trypan blue (Fig. 3*C* and Fig. S5). Counterstaining these postmortem sections with thioflavin S, a well-established amyloid stain, reveals that 100% of thioflavin S (ThioS)-positive plaques were labeled with Trypan blue from the PBCA NP injection (Fig. S5). This is a robust staining of Alzheimer pathology with PBCA NP-bound dye. Collectively, these data indicate that PBCA NPs can effectively deliver small BBB-impermeable targeted optical probes for in vivo neuroimaging.

We next sought to determine whether PBCA NPs can deliver therapeutic/imaging biological agents such as antibodies into the brain after peripheral injection. Thus, we coated PBCA-NPs with Alexa-488–conjugated anti-Aβ antibody (6E10), i.v. injected them into APP/PS1 mice, and used in vivo multiphoton microscopy to determine whether the antibodies cross the BBB. We found that Alexa-488–conjugated 6E10 antibodies cross the BBB upon adsorption onto PBCA NPs and stain amyloid plaques in the brains of APP/PS1 mice ($n = 5$) beginning at 15 min after injection and peaking at 2 h (Fig. 4). Aβ-antibody binding to senile plaques in the brain was confirmed postmortem by immunohistochemical secondary labeling with Cy3-conjugated antimouse IgG (Fig. 4). Control experiments in which Alexa-488–labeled anti-Aβ antibodies were i.v. injected without adsorption onto PBCA NPs showed no Alexa-488 signal in plaques after 2 h of imaging (Fig. 4). Postmortem immunostaining with a different anti-Aβ antibody (R1282) raised in rabbit and costaining with antimouse-488 to ensure all 6E10 PBCA NP signal was detected showed that 92.2% of R1282-stained plaques were also labeled by 6E10 (Fig. 4 *F*–*H*). The 7.8% of plaques that were not labeled by the 6E10 PBCA NPs

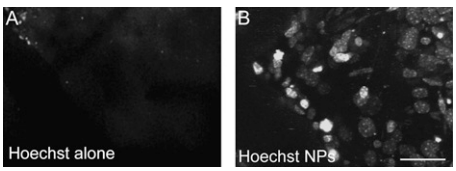

Fig. 1. PBCA NPs deliver BBB-impermeable fluorophores into mouse brain. In vivo two-photon imaging of the brain of wild-type mice reveals that PBCA NPs coated with polysorbate 80 efficiently deliver BBB-impermeable optical imaging fluorophores into the brain of living anesthetized mice. Hoechst alone dissolved in PBS does not cross the BBB after i.v. injection into mice (*A*), but upon adsorbing Hoechst onto PBCA NPs and coating with polysorbate 80, Hoechst crosses the BBB and stains nuclei in the brain beginning at 30 min and persisting over 24 h (*B*). (Scale bar, 15 μm.)

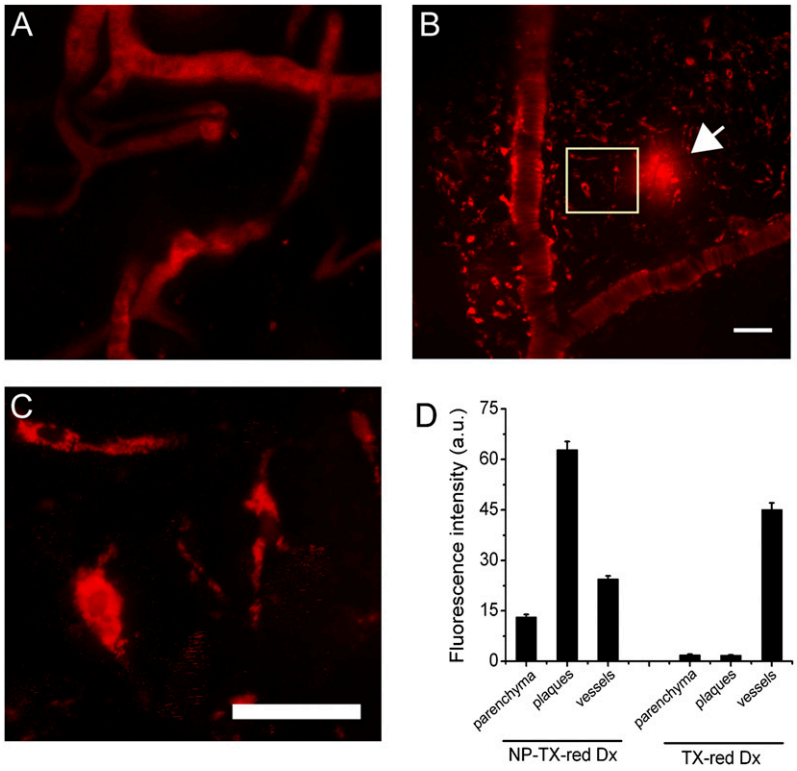

Fig. 2. Texas red dextran covalently linked to PBCA NPs crosses BBB and labels neuropathological changes of Alzheimer's disease. In vivo two-photon imaging of the brain of living mice ($APP_{swe}/PS1_{deltaE9}$) show that BBB-impermeable fluorophores covalently conjugated to PBCA NPs enter the brain and stain senile plaques, neuropathological lesions of AD. Administering Texas red dextran (70 kDa M_r) alone dissolved in PBS does not cross the BBB, remaining in blood vessels after 2 h following i.v. injection (*A*). On the contrary, covalently incorporating Texas red into PBCA NPs and coating NPs with polysorbate 80 allows them to cross the BBB and stain amyloid plaques (arrow), cerebral amyloid angiopathy, and neuronal/glial cell bodies (*B* and *C*). Quantification of fluorescence intensity in these experiments revealed a 10-fold increase of TX-red-Dx signal in the brain parenchyma and robust staining of amyloid plaques in vivo upon delivering the fluorophore using PBCA NPs compared with TX-red-Dx injected alone (*D*). (Scale bars in *B* and *C*, 20 μm.)

were small, with a diameter of <5 μm. This is slightly less robust than the 100% staining efficiency observed with Trypan blue PBCA NPs but still an impressive efficiency for a large biological molecule crossing the BBB. Together, these data suggest that PBCA NPs are not only effective at brain delivery of small targeted optical imaging dyes, but large biologic imaging/therapeutic antibodies as well.

Because optical imaging techniques such as multiphoton microscopy are generally very sensitive and can detect very weak fluorescence signals in scattering tissue, it is unclear whether PBCA NPs can be used to deliver sufficient amounts of targeted molecular imaging contrast agents for clinically relevant imaging technologies such as MRI, which requires substantial amounts of contrast agents to enter the brain for contrast enhancement. We therefore asked whether MRI contrast agents could be adsorbed onto PBCA NPs and delivered into the brain for in vivo neuroanatomical MR imaging. To address this question, we adsorbed gadobutrol (Gadovist)—a 605-Da MRI gadolinium (Gd)-based contrast agent routinely used in humans for imaging anatomical lesions—onto PBCA NPs and administered them into wild-type mice for neuroanatomical MRI. Moreover, we used inductively coupled plasma-mass spectroscopy (ICP-MS) to quantify the amount of gadolinium adsorbed onto PBCA NPs and delivered into the brain so that we could precisely determine the efficiency of BBB transport. We found that 2.5 h after i.v. injecting gadobutrol adsorbed onto PBCA NPs (10% adsorption efficiency), 5.34% of the injected nanoparticle-loaded gadolinium per gram of tissue remained in the brain compared with only 0.009% injected dose of free gadolinium per gram of tissue when gadobutrol is injected without PBCA NPs; this corresponds to several hundred fold increase in delivery of gadobutrol into the brain when PBCA NPs are used. ICP-MS measurements at longer time points confirmed that PBCA NP-loaded gadolinium was almost completely cleared from the brain within 24 h after injection (Table S1).

After confirming that substantial amounts of gadolinium get into the brain, we carried out serial T1-weighted gradient-echo imaging of the brain of injected mice over a 2-h time period to assess the kinetic properties of gadobutrol adsorbed PBCA NPs entering the brain upon i.v. administration. We find that PBCA NPs deliver gadobutrol into the brain with a brain parenchyma penetrating time constant of 19.5 min (kinetics follow monoexponential fit), which is very similar to that observed by in vivo two-photon microscopy using Trypan blue-loaded PBCA NPs (Fig. 5). We note that because the MRI signal depends on both the R1 relaxation rate (which is effected by the Gd concentration) as well as the experimental repetition time (TR), the significantly increased Gd concentration translates into a signal increase of only 1.5 fold for a TR of 600 ms (Fig. 5*C*). Whereas some of the observed signal increase in the MRI will be attributable to Gd in the blood due to the 2-h half-life of the PBCA nanoparticles, it will likely be a small contribution. First, the brain blood volume is only ~3%. Second, because the gadobutrol is sequestered inside the PBCA nanoparticle, the Gd relaxivity will depend on the water exchange across the dextran-coated PBCA nanoparticle surface and the encapsulated gadobutrol will likely be less effective at relaxing the bulk vascular water than free gadobutrol. This hypothesis is supported by the observed slow increase over time in the brain MRI signal (Fig. 5*C*) and the slow decrease over time of the T1 relaxation time (Fig. 5*D*), which can only be attributed to a slowly increasing Gd concentration. Because the Gd concentration in the blood vessels decreases by ~50% over the 2-h time period, the slowly decreasing T1 and increasing MRI signal can only be explained by a slow increase in the tissue Gd concentration. These data suggest the PBCA NPs enhance delivery of a clinically approved MRI contrast agent to the brain to an extent that is suitable for MR imaging, indicating the possibility of delivering targeted MRI contrast agents into the brain.

To more carefully characterize the cellular location of exogenous molecules delivered into the brain using PBCA NPs, we adsorbed 10 nm gold particles onto PBCA NPs and used TEM to image the brain after injection of PCBA NPs coated with 10 nm gold particles. We observed gold in endothelial cell cytoplasm, basal lamina, neuropil structures including synapses, neuronal soma, and glial soma, consistent with the multiphoton

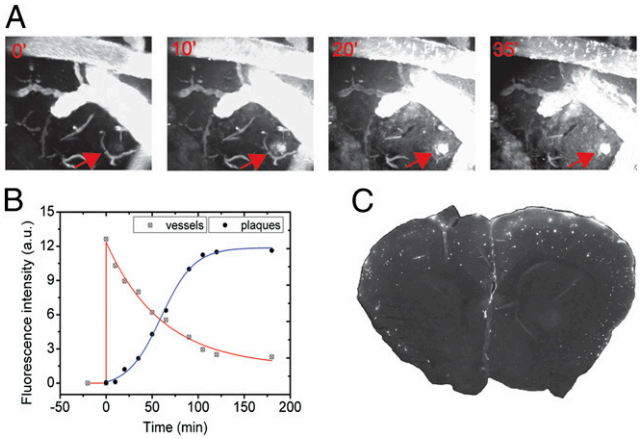

Fig. 3. Trypan blue delivered to brain of AD transgenic mouse using PBCA NPs. Four-dimensional in vivo multiphoton microscopy of the brain of living anesthetized AD transgenic mice ($APP_{swe}/PS1_{deltaE9}$) shows that PBCA NPs coated with polysorbate-80 deliver Trypan blue into the brain. Snapshots of the brains of AD transgenic mice injected with NPs loaded with Trypan blue obtained at the indicated times via in vivo two-photon microscopy are shown (*A*). Quantitative analysis of the kinetics of NP-mediated delivery of Trypan blue into the brain reveals an increase in Trypan blue fluorescence in plaques that follow a sigmoidal Boltzmann equation with time constants t_o = 18 min, corresponding to BBB crossing, and $\Delta\tau$ = 60 min, corresponding plaque labeling. The half-life of Trypan blue adsorbed onto NPs in the vessels is 61 min (*B*). Postmortem histological analysis reveals that Trypan blue delivered to the brain using NPs stains plaques throughout both cortical and subcortical regions of the brain.

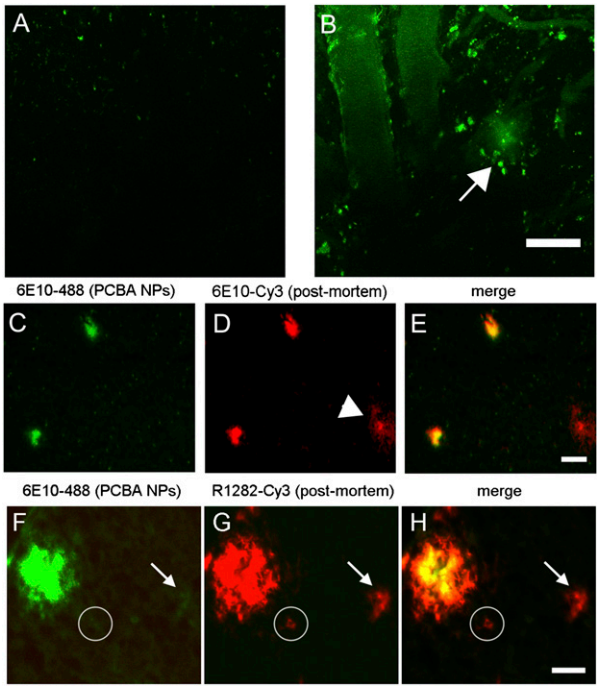

Fig. 4. PBCA NPs deliver fluorescently labeled Aβ antibodies into mouse brain. Aβ antibodies (6E10) conjugated to Alexa-488 were adsorbed onto PBCA NPs and injected i.v. into 6-mo-old APP/PS1 mice. In vivo two-photon imaging of brains was carried out 2 h after injecting PBCA NPs loaded with 6E10–Alexa-488. Administrating free 6E10–Alexa-488 antibodies i.v. and imaging the brain revealed no staining of senile plaques (*A*). Upon injecting PBCA NPs loaded with 6E10–Alexa-488, some fluorescence signal was detected in amyloid plaques (arrow) within the brain of APP/PS1 mice (*B*). Postmortem analysis of the brain of PBCA NPs injected animals reveals robust amyloid plaque staining (*C*), both with the labeled 6E10–Alexa-488 (green) and with a secondary antimouse IgG antibody labeled with Cy3 (red) (*D*). Of note, a subset of diffuse plaques was neither seen in vivo nor postmortem with 6E10–488, but was clearly seen upon addition of the Cy3 secondary antibody (arrowhead in *D*). Merge of *C* and *D* is shown in *E*. Immunostaining with a different Aβ antibody, R1282,and secondary antirabbit Cy3 and antimouse-488 (to detect all 6E10 injected with NPs), shows that the vast majority of plaques (92.2%) are labeled by 6E10 (*F–H*). Large plaques are very strongly labeled, whereas smaller plaques occasionally had only weak 6E10 staining (arrow) and 7.8% of plaques were unlabeled with 6E10. These unlabeled plaques were all <5 μm in diameter (circle). (Scale bars in *B* and *E*, 50 μm; in *H*, 20 μm.)

observations of widespread distribution of nanoparticles coated with fluorophores (Fig. S6). Gold particles were not observed in the brain of an animal injected with gold particles not adsorbed onto PBCA NPs. This finding confirms at an ultrastructural subcellular resolution that PBCA NPs effectively deliver exogenous BBB-impermeable molecules into the brain parenchyma.

Having demonstrated that PBCA NPs can effectively deliver molecular imaging dyes and biologic probes into the brain, we next wanted to determine the mechanism by which they cross the BBB. On the basis of size (~200 nm mean hydrodynamic diameter), it is very unlikely that PBCA NPs cross the BBB through passive paracellular diffusion. To determine whether PBCA NPs nonspecifically disrupt the BBB, as has been previously reported in a porcine in vitro model (23), we carried out three control experiments. First, we imaged the brains of living animals injected with two different dyes using in vivo multiphoton microscopy—first with Hoechst adsorbed onto PBCA NPs, and then with Texas red dextran (70 kDa M_r) in saline without NPs i.v. injected 30 min afterward. We found that Hoechst adsorbed onto PBCA NPs crossed the BBB and stained neuronal and glial nuclei in vivo, whereas Texas-red-Dx remained in cerebral blood vessels without evidence of substantial leakage (n = 5; Fig. 6*A*). In the inverse experiment, injection of Texas-red-Dx incorporated in PBCA NPs followed 30 min later by unbound 1 mM Hoechst-labeled plaques and neurons in APP/PS1 transgenic brain without any Hoechst labeling in the parenchyma (Fig. 6*A*, *Inset*). Second, we used dynamic contrast enhanced (DCE) MRI to visualize the brains of living intact wild-type mice to test whether PBCA NPs induce BBB leakage of gadolinium-dithylenetiamine penta-acetic acid (Gd-DTPA, 545.6 Da M_r), a BBB-impermeable MR contrast agent used to assess cerebral vascular integrity. DCE-MRI sequences were performed 30 min following i.v. administration of PBCA NPs loaded with Hoechst (n = 3 mice). DCE MR images revealed strong Gd-DTPA signal enhancement in blood vessels and muscle tissue within minutes after injection (Fig. 6 *B* and *C*), but no increase in Gd-DTPA–induced signal intensity changes in the brain. Third, we examined the BBB of animals that had been injected with nanoparticles coated with 10 nm colloidal gold using TEM and found that the BBB appears structurally completely normal (Fig. 6*D*). Together these results show that PBCA NPs cross the BBB without inducing nonspecific disruption of the BBB in the intact brain in contrast to data derived from an in vitro model of the BBB (23).

We next wanted to identify molecular candidates that may be involved in transporting PBCA NPs across the BBB. It has been hypothesized that biodegradable nanoparticles adsorb apolipoprotein E (apoE) particles in plasma onto their surfaces and cross the BBB via receptor-mediated transcytosis (24). To determine whether or not apoE is necessary for PBCA NPs to cross the BBB, we i.v. injected Hoechst-encapsulated PBCA NPs into APOE knockout ($APOE^{-/-}$) mice and then used multiphoton microscopy to image the brain in vivo. We find the Hoechst-loaded polysorbate-80 coated PBCA NPs do not cross the BBB in $APOE^{-/-}$ mice (n = 3; Fig. 6*E*). However, preincubating Hoechst-loaded PBCA NPs in lipidated apoE particles for 2 h at 25 °C before injecting the NPs i.v. into $APOE^{-/-}$ mice allowed them to cross the BBB, releasing Hoechst to robustly stain neuronal/glial nuclei

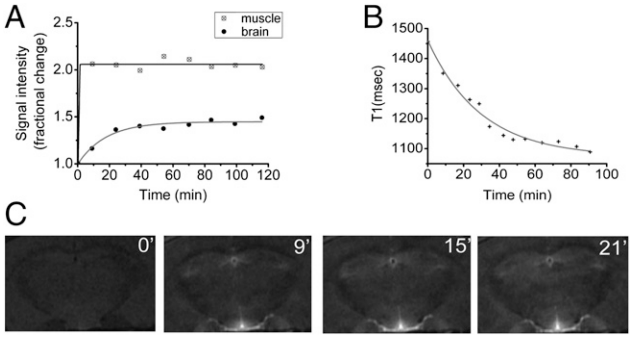

Fig. 5. PBCA NPs enhance delivery of MRI contrast agent into the brain. Serial signal intensity measurements of T1 gradient-echo MR images of wild-type mouse brain before and after i.v. administration of polysorbate 80-coated PBCA NPs loaded with gadobutrol reveal contrast enhancement of brain parenchyma over time. Whereas gadobutrol enters muscles almost instantaneously upon delivery with nanoparticles, the kinetics of gadobutrol signal in the brain followed a monoexponential model with a time constant of ~19 min (*A*). T1 decreased by ~25% over 2 h with kinetics that followed a monoexponential decay [$T_1 = 1074 + 386*\exp(-t/\tau)$; time constant $\tau = 29.7$ min] (*B*). Sample T1 gradient-echo images showing an increase in gadobutrol signal in the brain over time is also shown (*C*).

(Fig. 6*E*). These findings support the hypothesis that PBCA NPs cross the BBB through a mechanism that involves the adsorption of apoE from plasma, making receptor-mediated transcytosis through vascular endothelial cells the likely mechanism by which PBCA NPs cross the BBB.

Discussion

Breakthroughs in molecular imaging continue to revolutionize medicine and biological research, yet one area that has been challenging involves imaging molecular targets in the brain in real-time, in part due to difficulties in developing contrast agents with target specificity that also cross the BBB. Enhancing delivery of BBB-impermeable contrast agents and molecular imaging probes therefore has the potential to greatly increase the utility of imaging techniques for visualizing specific targets in the brain. We investigated the use of nanocarrier systems, specifically PBCA NPs coated with polysorbate 80, for delivering BBB-impermeable molecular imaging contrast agents into the brain. We demonstrated that (*i*) PBCA NPs can efficiently and safely deliver BBB-impermeable optical molecular imaging fluorophores into the brain in mice to allow in vivo imaging of neuronal and glial nuclei; (*ii*) PBCA NPs can serve as nanocarriers for transporting BBB-impermeable targeted fluorophores for imaging neuropathological changes in a neurodegenerative disease, Alzheimer's; (*iii*) PBCA NPs can be used to deliver biologics such as antibodies into the brain; and (*iv*) PBCA NPs can deliver sufficient amounts of BBB-impermeable molecular contrast agents to allow imaging of the brain using clinically relevant techniques such as MRI with improved signal-to-noise ratio. Using 4D multiphoton microscopy, DCE-MRI, and ICP-MS, we carefully studied the kinetics of PBCA NPs-mediated delivery of BBB-impermeable molecules into the brain and found that NPs deliver >5% of nanoparticle-adsorbed administered dose of BBB-impermeable molecular probes into the brain with a time constant of ~18 min. We further show that PBCA NPs do not induce nonspecific disruption of the BBB, but cross the BBB using a mechanism that requires endogenous apoE, suggesting that PBCA NPs are a safe and viable approach for delivering BBB-impermeable molecules into the brain.

Several nonnanotechnology-based methods have been investigated to noninvasively deliver BBB-impermeable molecules into the brain. Approaches involving nonspecifically disrupting the BBB using hypertonic osmotic agents, bradykinins, and

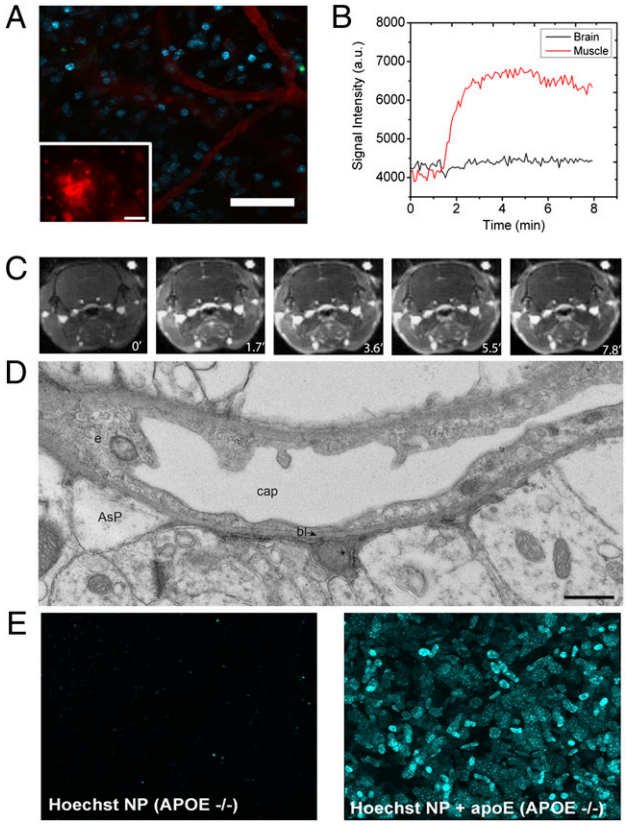

Fig. 6. PBCA NPs do not induce nonspecific BBB disruption but require apoE to cross BBB. Injecting PBCA NPs loaded with Hoechst and then injecting Texas red dextran dissolved in PBS (not on NPs) 30 min afterward and imaging the brain through a cranial window using in vivo two-photon microscopy reveals robust Hoechst staining of nuclei without leakage of Texas red dextran into the brain (*A*). Conversely, injecting Texas red dextran incorporated into PBCA NPs followed 30 min later by unbound Hoechst resulted in plaque and intraneuronal labeling with Texas red and no parenchymal Hoechst labeling (*A*, *Inset*). Dynamic contrast enhanced MRI sequence consisting of 100 repetitions of T1-weighted gradient-echo sequence with a temporal resolution of 4.8 s in the brains of mice injected with Gd-DTPA 30 min after PBCA NPs loaded with Hoechst were i.v. injected reveals robust increase of Gd-DTPA signal intensity in muscle but not the brain, suggesting that PBCA NPs do not induce nonspecific disruption of the BBB (*B* and *C*). In animals injected with nanoparticles, TEM confirms an intact BBB with normal endothelial cells (e), basal lamina (bl), and astrocytic processes (AsP) surrounding capillaries (cap) (*D*). Unlike wild-type mice, APOE knockout mice i.v. injected with polysorbate 80-coated PBCA NPs loaded with Hoechst did not have robust nuclei staining with Hoechst >2 h after NP injection (*E*). Preincubating Hoechst-loaded PBCA NPs with astrocyte-secreted apoE particles for 2 h and then i.v. administering NPs into APOE knockout mice allowed Hoechst to cross the BBB, robustly staining neuronal and glial nuclei (*E*). Images in *E* represent a *z*-projection of a stack of seven images. [Scale bar, 100 μm (*A*), 20 μm (*A*, *Inset*), 500 nm (*D*).]

alkylglycerols have all been demonstrated to be effective at enhancing delivery of BBB-impermeable drugs into the brain (25–30). Focused ultrasound beams (FUSB), electromagnetic radiation (EMR), and recently focused pulsed laser disruption of vessel walls have also been used to disrupt the BBB to enhance delivery of fluorophores into the brain with some success (22, 31–34). However, all of these chemical and mechanical approaches nonspecifically disrupt BBB integrity; thus, their use for molecular imaging is limited because they increase the influx of toxins into the brain and influence CNS biology in ways that cannot be adequately controlled.

The use of nanotechnology to transport exogenous molecules into the brain provides a simple and effective alternative approach

(35). Most previous studies using nanoparticulate delivery systems for getting BBB-impermeable compounds into the brain have focused on drug delivery. For instance, multiple studies have shown that PBCA NPs can be used to deliver a variety of small polar drugs into the brain (10–13, 35, 36). In all of these studies, however, the level of brain delivery of exogenous molecules was not directly visualized in real time, but instead indirect reporters such as assessing drug effects were used to evaluate BBB crossing. We took advantage of advanced molecular imaging techniques to directly demonstrate that PBCA NPs can be used to deliver targeted BBB-impermeable contrast agents into the brain in sufficient amounts to allow in vivo optical imaging of cellular and neuropathological structures and BBB penetration of MR contrast agents in the brain of living mice. We characterize the kinetics of PBCA NPs-mediated BBB crossing as well as the amount of exogenous molecules delivered to the brain upon loading onto PBCA NPs and also demonstrate that PBCA NPs require adsorption of plasma apoE to cross the BBB. Future studies will be able to apply this technology to a wide variety of imaging modalities that will be useful in animal and human brain including near infrared imaging and using targeted MR probes. We anticipate that these findings will provide a technique to allow advances in in vivo neuroimaging at the cellular and systems level by helping to overcome the challenges posed to contrast agent and ligand development by the BBB.

Materials and Methods

Preparation and Characterization of Nanoparticles. All protocols for preparing and characterizing poly(*N*-butyl cyanoacrylate) nanoparticles are outlined in *SI Materials and Methods*.

Transmission Electron Microscopy. All details for TEM experiments are as outlined in *SI Materials and Methods*.

Animal Surgeries and Imaging. Detailed surgery and imaging protocols are outlined in *SI Materials and Methods*.

Inductively Coupled Plasma-Mass Spectroscopy. Detailed procedures for ICP-MS are outlined in *SI Materials and Methods*.

Magnetic Resonance Imaging Experiments. Dynamic contrast enhanced MRI and serial T1-weighted MRI experimental protocols are as detailed in *SI Materials and Methods*.

ACKNOWLEDGMENTS. We thank Dr. Marian DiFiglia for use of the transmission electron microscope and Dr. Peter Caravan for the use of the ICP-MS. This work was supported by National Institutes of Health (NIH) Grants K99 AG033670, K25 AG029415, K08 NS069811, P50 AG005134, AG12406, and AG08487, and a Coins for Alzheimer's Research Trust award. R.M.K. is supported by the Harvard Biophysics and Medical Scientist Training Programs (NIH T32 GM07753) and the Paul and Daisy Soros Foundation. L.-J.S. is supported by the Foundation Family Klee Young Scientist Award.

1. Backskai BJ, et al. (2003) Four-dimensional multiphoton imaging of brain entry, amyloid binding, and clearance of an amyloid-beta ligand in transgenic mice. *Proc Natl Acad Sci USA* 100:12462–12467.
2. Backskai BJ, Klunk WE, Mathis CA, Hyman BT (2002) Imaging amyloid-beta deposits in vivo. *J Cereb Blood Flow Metab* 22:1035–1041.
3. Klunk WE, et al. (2002) Imaging Abeta plaques in living transgenic mice with multiphoton microscopy and methoxy-X04, a systemically administered Congo red derivative. *J Neuropathol Exp Neurol* 61:797–805.
4. Ono M, Saji H (2011) SPECT imaging agents for detecting cerebral β-amyloid plaques. *Int J Mol Imaging* 2011:543267.
5. Svoboda K, Yasuda R (2006) Principles of two-photon excitation microscopy and its applications to neuroscience. *Neuron* 50:823–839.
6. Spires-Jones TL, de Calignon A, Meyer-Luehmann M, Backskai BJ, Hyman BT (2011) Monitoring protein aggregation and toxicity in Alzheimer's disease mouse models using in vivo imaging. *Methods* 53:201–207.
7. McLellan ME, Kajdasz ST, Hyman BT, Backskai BJ (2003) In vivo imaging of reactive oxygen species specifically associated with thioflavine S-positive amyloid plaques by multiphoton microscopy. *J Neurosci* 23:2212–2217.
8. Neuwelt EA, et al. (2011) Engaging neuroscience to advance translational research in brain barrier biology. *Nat Rev Neurosci* 12:169–182.
9. Bhaskar S, et al. (2010) Multifunctional nanocarriers for diagnostics, drug delivery and targeted treatment across blood-brain barrier: Perspectives on tracking and neuroimaging. *Part Fibre Toxicol* 7:3.
10. Kreuter J, Alyautdin RN, Kharkevich DA, Ivanov AA (1995) Passage of peptides through the blood-brain barrier with colloidal polymer particles (nanoparticles). *Brain Res* 674:171–174.
11. Alyautdin RN, et al. (1998) Significant entry of tubocurarine into the brain of rats by adsorption to polysorbate 80-coated polybutylcyanoacrylate nanoparticles: An in situ brain perfusion study. *J Microencapsul* 15:67–74.
12. Alyautdin RN, et al. (1997) Delivery of loperamide across the blood-brain barrier with polysorbate 80-coated polybutylcyanoacrylate nanoparticles. *Pharm Res* 14:325–328.
13. Friese A, Seiller E, Quack G, Lorenz B, Kreuter J (2000) Increase of the duration of the anticonvulsive activity of a novel NMDA receptor antagonist using poly(butylcyanoacrylate) nanoparticles as a parenteral controlled release system. *Eur J Pharm Biopharm* 49:103–109.
14. Tian XH, et al. (2011) Enhanced brain targeting of temozolomide in polysorbate-80 coated polybutylcyanoacrylate nanoparticles. *Int J Nanomedicine* 6:445–452.
15. de Calignon A, et al. (2010) Caspase activation precedes and leads to tangles. *Nature* 464:1201–1204.
16. Hardy J, Selkoe DJ (2002) The amyloid hypothesis of Alzheimer's disease: Progress and problems on the road to therapeutics. *Science* 297:353–356.
17. Koffie RM, et al. (2009) Oligomeric amyloid beta associates with postsynaptic densities and correlates with excitatory synapse loss near senile plaques. *Proc Natl Acad Sci USA* 106:4012–4017.
18. Li S, et al. (2009) Soluble oligomers of amyloid Beta protein facilitate hippocampal long-term depression by disrupting neuronal glutamate uptake. *Neuron* 62:788–801.
19. Cleary JP, et al. (2005) Natural oligomers of the amyloid-beta protein specifically disrupt cognitive function. *Nat Neurosci* 8:79–84.
20. Lacor PN, et al. (2007) Abeta oligomer-induced aberrations in synapse composition, shape, and density provide a molecular basis for loss of connectivity in Alzheimer's disease. *J Neurosci* 27:796–807.
21. Skowronek M, et al. (2000) The conformational characteristics of Congo red, Evans blue and Trypan blue. *Comput Chem* 24:429–450.
22. Raymond SB, et al. (2008) Ultrasound enhanced delivery of molecular imaging and therapeutic agents in Alzheimer's disease mouse models. *PLoS ONE* 3:e2175.
23. Rempe R, Cramer S, Hüwel S, Galla H-J (2011) Transport of Poly(n-butylcyano-acrylate) nanoparticles across the blood-brain barrier in vitro and their influence on barrier integrity. *Biochem Biophys Res Commun* 406:64–69.
24. Kreuter J, et al. (2002) Apolipoprotein-mediated transport of nanoparticle-bound drugs across the blood-brain barrier. *J Drug Target* 10:317–325.
25. Neuwelt EA, et al. (1991) Primary CNS lymphoma treated with osmotic blood-brain barrier disruption: Prolonged survival and preservation of cognitive function. *J Clin Oncol* 9:1580–1590.
26. Neuwelt EA, Pagel MA, Dix RD (1991) Delivery of ultraviolet-inactivated 35S-herpesvirus across an osmotically modified blood-brain barrier. *J Neurosurg* 74:475–479.
27. Rapoport SI (2000) Osmotic opening of the blood-brain barrier: Principles, mechanism, and therapeutic applications. *Cell Mol Neurobiol* 20:217–230.
28. Lee HJ, Zhang Y, Pardridge WM (2002) Blood-brain barrier disruption following the internal carotid arterial perfusion of alkyl glycerols. *J Drug Target* 10:463–467.
29. Erdlenbruch B, et al. (2003) Alkylglycerol opening of the blood-brain barrier to small and large fluorescence markers in normal and C6 glioma-bearing rats and isolated rat brain capillaries. *Br J Pharmacol* 140:1201–1210.
30. Emerich DF, Dean RL, Osborn C, Bartus RT (2001) The development of the bradykinin agonist labradimil as a means to increase the permeability of the blood-brain barrier: From concept to clinical evaluation. *Clin Pharmacokinet* 40:105–123.
31. Schirmacher A, et al. (2000) Electromagnetic fields (1.8 GHz) increase the permeability to sucrose of the blood-brain barrier in vitro. *Bioelectromagnetics* 21:338–345.
32. Cho CW, et al. (2002) Ultrasound-induced mild hyperthermia as a novel approach to increase drug uptake in brain microvessel endothelial cells. *Pharm Res* 19:1123–1129.
33. Raymond SB, Skoch J, Backskai BJ, Hynynen K (2007) Modular design for in vivo optical imaging and ultrasound treatment in the murine brain. *IEEE Trans Ultrason Ferroelectr Freq Control* 54:431–434.
34. Raymond SB, Skoch J, Hynynen K, Backskai BJ (2007) Multiphoton imaging of ultrasound/Optison mediated cerebrovascular effects in vivo. *J Cereb Blood Flow Metab* 27:393–403.
35. Kreuter J (1995) Nanoparticulate systems in drug delivery and targeting. *J Drug Target* 3:171–173.
36. Aliautdin RN, Petrov VE, Ivanov AA, Kreuter J, Kharkevich DA (1996) Transport of the hexapeptide dalargin across the hemato-encephalic barrier into the brain using polymer nanoparticles. *Eksp Klin Farmakol* 59:57–60.